ISSN 1064-2269, Journal of Communications Technology and Electronics, 2006, Vol. 51, No. 10, pp. 1154–1168. © Pleiades Publishing, Inc., 2006.
Original Russian Text © A.S. Bugaev, I.A. Vasil'ev, S.I. Ivashov, V.V. Chapurskii, 2006, published in Radiotekhnika i Elektronika, 2006, Vol. 51, No. 10, pp. 1224–1239.

THEORY AND METHODS OF SIGNAL PROCESSING

Radar Methods of Detection of Human Breathing and Heartbeat

A. S. Bugaev, I. A. Vasil'ev, S. I. Ivashov, and V. V. Chapurskii

Received March 29, 2006

Abstract—Methods of extracting information from observations of human subjects by short-range radars with various types of probing signals are theoretically analyzed. The time and frequency features of breathing and heartbeat realizations obtained by different demodulation methods from monochromatic and video-pulse probing signals are considered. Algorithms for discrimination of signals reflected by human objects from interfering reflections from local objects are modeled for continuous probing signals with stepwise frequency modulation.

PACS numbers: 87.16.Xa, 84.40.Ba

DOI: 10.1134/S1064226906100056

INTRODUCTION

In the last ten years, much interest has been shown in radar methods for detecting a human subject as a whole or for examining a particular internal part of a human organism [1–13]. Detection of a human being as a living object can be performed by short-range radars, which can use microwave signals ranging in frequency, waveform, duration, and bandwidth. Potential applications of short-range radars are, for example, the following:

(i) detection of alive human persons under debris of buildings destroyed as a result of natural disasters or man-made catastrophes [2, 4, 11];

(ii) detection of people and parameters of their motion inside buildings or outdoors under low-visibility conditions (because of poor weather, sight obstructions, etc.) in antiterrorist operations [1, 2, 4, 5, 8, 11];

(iii) examination of transport containers for revealing illegal persons [2];

(iv) remote diagnostics of a person's emotional state during latent or open checks in criminal investigations or at checkpoints, as well as within manned machine systems [2];

(v) remote detection of verbal signals [3].

In addition, various medical applications should be mentioned:

(i) contactless measurement of parameters of heartbeat and breathing for patients for whom contact gauges cannot be used [1, 2, 6, 8];

(ii) measurement of heart rate variability in heart disease diagnostics [6, 12];

(iii) estimation of vessel elasticity from pulse-wave velocity for revealing patients predisposed to cardiovascular disease [12];

(iv) internal diagnostics [6].

Among signals suitable for detecting a living object are continuous modulated or unmodulated microwave signals at frequencies ranging from hundreds of megahertz to tens of gigahertz; narrowband, wideband, or ultrawideband (UWB) signals; and video-pulse signals that have no clearly defined carrier frequency [4–8, 13, 14].

Being reflected from a human object, a signal acquires specific biometrical modulation, which does not appear in the case of reflection from inanimate local objects. This specific modulation is produced by heartbeats, pulsations of vessels, lungs, and, especially, by skin vibrations in the region of thorax and larynx, which occur synchronously with breathing motions and heartbeat [1–2, 6]. These processes are nearly periodic with typical frequencies in the range of 0.8–2.5 Hz for heartbeat and 0.2–0.5 Hz for breathing. Therefore, the delay or phase of the reflected signal is periodically modulated by oscillations of skin and internals. The modulation parameters are determined by the frequencies and intensities of respiration and heartbeat. Aperiodic modulations may also originate from small motions of body parts and articulation when making the speech sounds [3, 8].

By applying the rejection method to probing signals and signals reflected from local objects, it is possible to attain high sensitivity in detecting objects whose boundaries perform mechanical vibrations. According to published data, the sensitivity of radar probing in the gigahertz band may theoretically reach 10^{-9} m [15].

In practice, radar probing of live persons is performed against the background of reflections from local objects. As a rule, the intensity of these reflections exceeds the intensity of signals from a human object. The latter, however, are distinguished by periodic and aperiodic modulation synchronous with the respiration and heartbeat of a person. Modulation of this type is either absent in signals reflected from local objects or

has different time and spectral characteristics. This is the key point which lays the basis for recognition of signals reflected by a human person against the background reflections from local objects. The main advantage of wideband and UWB signals over unmodulated signals in probing live objects is that the field under observation can be divided into distance cells; such a division makes it possible to measure the distance to a target and to improve its extraction from the background.

Generally, different types of probing signals may be advantageous for examining live objects depending on the essence of a particular problem. To date, most studies have dealt with only specific radar systems using probing signals of certain types and no attempt at comparative analysis has been made. The aim of this study is to analyze and compare the methods of data extraction that are used in radar systems with different types of signals. In particular, the characteristics of biometric signals and appropriate demodulation methods are compared for probing signals of the following types: an unmodulated monochromatic signal (MS), a UWB video-pulse signal, and a stepwise frequency modulated (SFM) waveform. In the last case, algorithms for detection and extraction of the breathing and heartbeat components in the presence of background reflections from local objects are synthesized.

1. PROBING LIVE OBJECTS BY MONOCHROMATIC RADARS

Despite a known disadvantage of unmodulated probing signal—the absence of range selection—radar sensors operating with this type of signals can widely be used in simple devices intended for detection of human respiration and heartbeat. Much work on the design and performance analysis of such sensors remains to be done, including

(i) analysis of nonlinear distortions appearing in a periodic pattern of breathing and heartbeat because of the phase modulation that a probing signal acquires when reflected from the boundaries of a human body, as well as when being transformed in the receiver;

(ii) comparison of the time and spectral output effects for the amplitude and quadrature reception schemes with having the possibility of estimating the variable phase of the received signal.

Let a monochromatic probing signal with amplitude U_0 and frequency ω_0 be written in a complex form,

$$\dot{u}_0(t) = U_0 \exp(j\omega_0 t). \quad (1)$$

Assume that the main part of reflection is observed at the air–skin interface. Let the range of skin surface reflections and vibrations be located within one Fresnel zone spaced at average distance r_0 from the sensor. Then, the current distance to the skin boundary can be written as

$$r(t) = r_0 + \Delta r(t), \quad (2)$$

where $\Delta r(t)$ characterizes skin-surface vibrations.

In view of (2), received signal $\dot{u}(t)$ is not only attenuated by factor q, but its phase also changes by the value $\varphi(t) = -2kr(t)$,

$$\dot{u}(t) = qU_0 \exp\{j\omega_0 t - j\psi_0 - j2k\Delta r(t)\}, \quad (3)$$

where $k = 2\pi/\lambda$ is the wavenumber, λ is the wavelength, and $\psi_0 = 2kr_0$.

Along with the desired signal, a so-called penetrating signal from the transmitter also appears at the receiver input, so that the total received signal has the form

$$\begin{aligned}\dot{u}_\Sigma(t) &= U_0[q_0 \exp(j\omega_0 t - j\varphi_0) \\ &+ q\exp(j\omega_0 t - j\psi_0 - j2k\Delta r(t))],\end{aligned} \quad (4)$$

where q_0 and q are the attenuation factors of the penetrating and desired signals, respectively, and φ_0 is the phase of the penetrating signal (taken below to be zero, $\varphi_0 = 0$).

For simplicity, let the periodic vibrations of the body surface due to breathing and heartbeat be represented as the sum of two harmonic functions:

$$\Delta r(t) = \Delta_{br}\sin(\omega_{br}t) + \Delta_{hb}\sin(\omega_{hb}t + \varphi_{hb}), \quad (5)$$

where $\omega_{br} = 2\pi F_{br}$; $\omega_{hb} = 2\pi F_{hb}$; F_{br}, F_{hb}, Δ_{br}, and Δ_{hb} are the frequencies and amplitudes of breathing and heartbeat, respectively; and φ_{hb} is a constant phase.

A radar sensor with an unmodulated probing signal may incorporate a receiving device of either of two types: a coherent quadrature receiver and a common amplitude receiver.

A coherent quadrature receiver. This receiver extracts two quadrature components of signal (4), which can be represented in the form of a complex amplitude [9]:

$$\dot{U}_\Sigma(t) = q_0U_0[1 + \alpha\exp(-j\psi_0 - j2k\Delta r(t))], \quad \text{where} \quad \alpha = q/q_0. \quad (6)$$

Having eliminated the constant component of the penetrating signal and taking into account expression (5), we

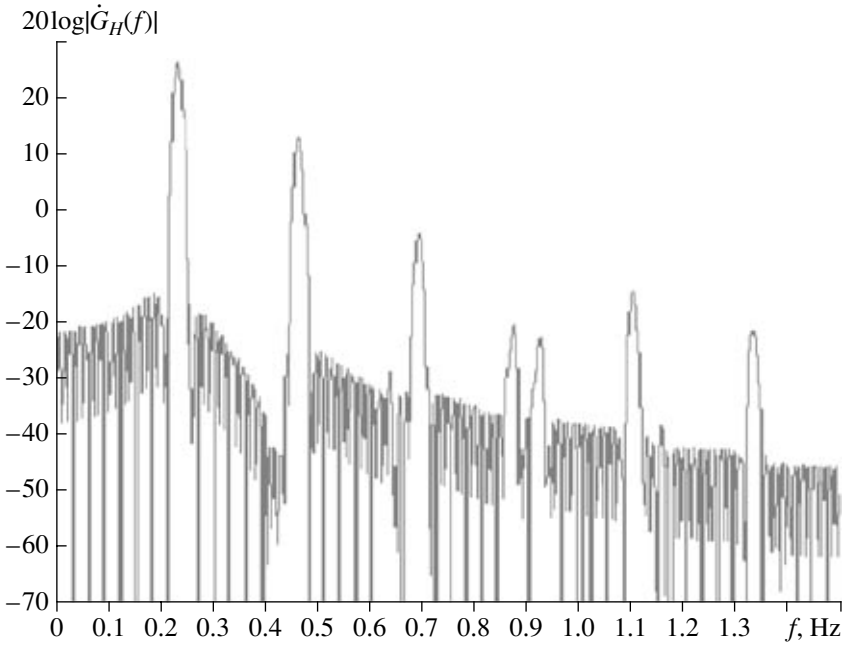

Fig. 1. Absolute value of the spectrum of the signal at the output of a radar sensor with coherent quadrature reception for the breathing and heartbeat frequencies 0.23 and 1.10 Hz, respectively.

obtain the normalized complex amplitude of the desired signal in the form

$$\dot{U}(t) = \exp\{-j\psi_0 - j2k(\Delta_{\text{br}}\sin(\omega_{\text{br}}t) + \Delta_{\text{hb}}\sin(\omega_{\text{hb}}t + \varphi_{\text{hb}}))\}. \quad (7)$$

Expanding the exponential factors in (7) in terms of Bessel functions $J_m(x)$ and assuming that process (7) is centered and weighted over a finite time interval ($-T/2$, $T/2$), we calculate its Fourier spectrum:

$$\dot{G}_H(\omega) = \exp(-j\psi_0)\{\dot{G}(\omega) - \bar{\dot{U}}W_H(\omega)\}, \quad (8)$$

where $\bar{\dot{U}}$ and $\dot{G}(\omega)$ are the average value and the spectrum of process (7) at the interval ($-T/2$, $T/2$),

$$\bar{\dot{U}} = \sum_{m_1, m_2 = -\infty}^{\infty} J_{m_1}(2k\Delta_{\text{br}})J_{m_2}(2k\Delta_{\text{hb}}) \times \exp(-jm_2\varphi_{\text{hb}})\text{sinc}((m_1\omega_{\text{br}} + m_2\omega_{\text{hb}})T/2\pi), \quad (9)$$

$$\dot{G}(\omega) = \sum_{m_1, m_2 = -\infty}^{\infty} J_{m_1}(2k\Delta_{\text{br}})J_{m_2}(2k\Delta_{\text{hb}}) \times \exp(-jm_2\varphi_{\text{hb}})W_H(m_1\omega_{\text{br}} + m_2\omega_{\text{hb}} + \omega). \quad (10)$$

In the above expression, $W_H(\omega)$ is the Fourier spectrum of the weight function. In the case of the generalized Hamming window [16],

$$W_H(\omega) = T\left\{a\,\text{sinc}\left(\frac{\omega T}{2\pi}\right) + \frac{1-a}{2}\left[\text{sinc}\left(\frac{\omega T}{2\pi} - 1\right) + \text{sinc}\left(\frac{\omega T}{2\pi} + 1\right)\right]\right\}, \quad (11)$$

where $\text{sinc}(x) = \sin(\pi x)/\pi x$.

Spectrum (8) contains harmonics with frequencies of breathing ω_{br} and heartbeat ω_{hb} as well as mixed and multiple harmonics with the frequencies $m_1\omega_{\text{br}} + m_2\omega_{\text{hb}}$. A harmonic's amplitudes can be found as the product of two Bessel functions of the arguments $2k\Delta_{\text{br(hb)}} = 4\pi\Delta_{\text{br(hb)}}/\lambda$, which are proportional to the respective displacements of the body surface in relation to the wavelength of the probing signal. It follows from (8) that, in the case of a coherent quadrature reception, the absolute value of the Fourier spectrum of the desired signal is independent of ψ_0 and, therefore, of average distance r_0 to the object.

Figure 1 gives an example of the absolute value of spectrum (8) calculated in the case of a simple Hamming window ($a = 0.54$) for the following values of the parameters: frequencies and amplitudes of skin vibrations due to breathing and heartbeat $F_{\text{br}} = \omega_1/2\pi = 0.23$ Hz, $\Delta_{\text{br}} = 1$ cm, $F_{\text{hb}} = \omega_2/2\pi = 1.1$ Hz, and $\Delta_{\text{hb}} =$

0.1 mm, respectively, and an operating frequency $f_0 = \omega_0/2\pi = 2.0$ GHz. The resolution of spectral analysis is 0.01 Hz in accordance with the chosen time of analysis $T = 100$ s. The plot in Fig. 1 correlates well with the spectrum of phase modulation of signal (7). The calculation also shows that the spectral composition of a signal received by a coherent quadrature receiver is not only independent of the average distance to the object but is almost independent of phase difference φ_{hb} between breathing and heartbeat signals.

Figure 2 plots two quadrature components at the receiver output obtained when a reflecting human object is situated at various distances and the distance phase takes the values $\psi_0 = 0°$, 45°, and 90°, all other parameters being the same as above. It is seen that the second harmonic of breathing, which is present in the cosine component at the distance phase $\psi_0 = 0°$, gradually vanishes from this component and transits to the sine component as the phase increases to $\psi_0 = 90°$, whereas the complex signal generally retains its spectrum, which is similar to that shown in Fig. 1. The third curve in the figures shows the argument of complex signal (7) after the subtraction of constant phase $\Phi(t) = -\arg(\dot{U}(t)) - \psi_0$; the variable component of this argument does not depend on ψ_0 and complies entirely with the model $\Delta\varphi(t) = -2k\Delta r(t)$, where $\Delta r(t)$ is taken in the form of (5).

Thus, to demodulate without distortion signal (7) of a monochromatic radar sensor and, thus, to extract breathing and heartbeat realizations, the signal should be subjected to coherent quadrature processing with determination of its phase samples. At high signal-to-noise ratios, this can be done by processing the quadratures in digital form and calculating phase sample values of the phase as an argument of complex amplitude (7). In the presence of noise, this problem can be solved on the basis of phase demodulators with phase-lock frequency control at an optimally chosen frequency characteristic of the phase-lock loop [17].

Amplitude receiver. This variant of signal processing is simpler and is considered here in view of its application in radar sensors of the RASCAN type [18], which have been used not only for detection of subsurface objects but also in experiments on probing live objects [8]. Assume that the detector has an approximately quadratic characteristic and there is a penetrating signal of the transmitter. Then, taking into consideration (4), equality $\varphi_0 = 0$, and the smallness of α ($\alpha \ll 1$), the voltage at the detector output can be represented in the form

$$u_{\text{det}}(t) = |\dot{u}_\Sigma(t)|^2 = q_0^2 U_0^2 |1 + \alpha\dot{U}(t)|^2 \approx q_0^2 U_0^2 \{1 + 2\alpha\text{Re}[\dot{U}(t)]\}. \quad (12)$$

We have determined the Fourier spectrum for the process $u_{\text{det}0}(t) = u_{\text{det}}(t)/(q_0^2 U_0^2)$, which is centered and weighted according to the Hamming algorithm as in the previous case:

$$\dot{G}_{H\text{det}}(\omega) = \alpha\{\dot{G}_H(\omega) + \dot{G}_H^*(-\omega)\}. \quad (13)$$

The calculation is carried out in accordance with formulas (8)–(10). It follows from (13) that the absolute

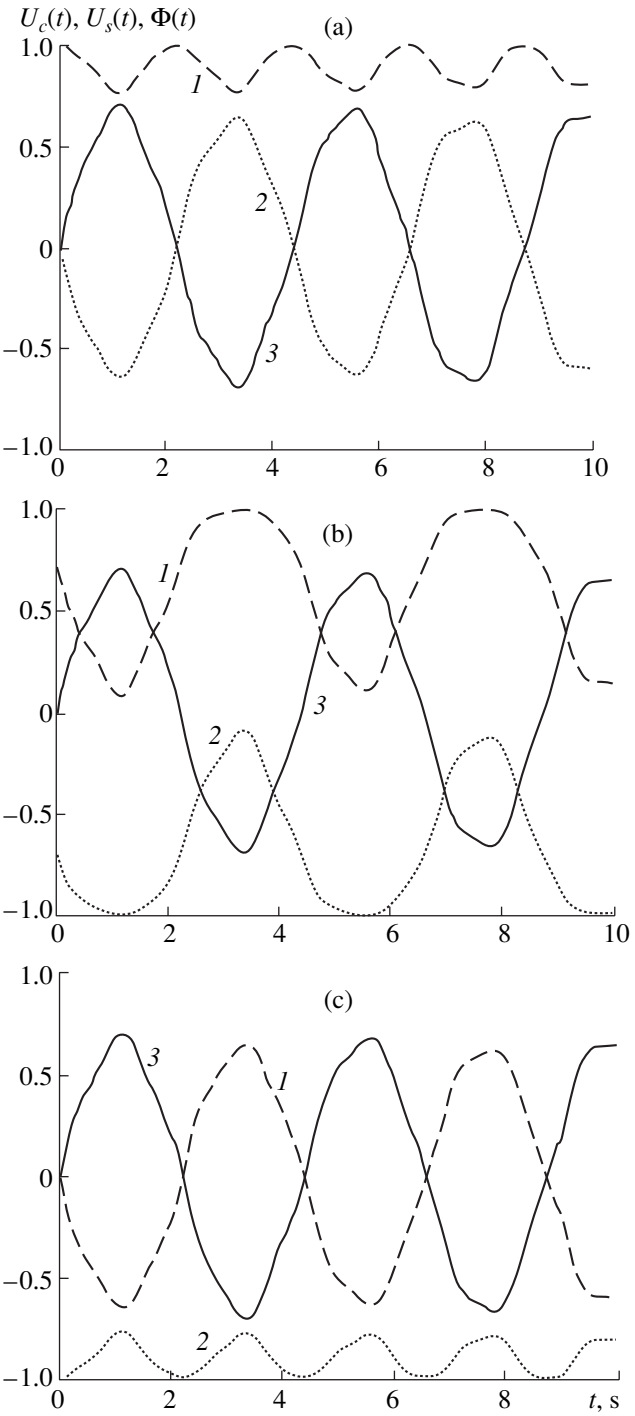

Fig. 2. Time realizations of (*1*, *2*) the quadrature components and (*3*) argument of the correlation integral for the distance phase ψ_0 = (a) 0°, (b) 45°, and (c) 90°.

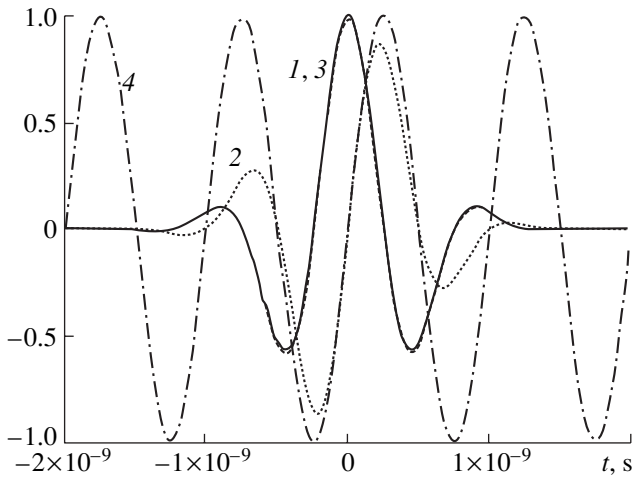

Fig. 3. Models of video-pulse probing signals: (*1*) $s_0(t)$, (*2*) $s_1(t)$, (*3*) $s_2(t)$, and (*4*) a monochromatic signal.

value of spectrum $|\dot{G}_{H\text{det}}(\omega)|$ depends on distance phase ψ_0, i.e., on average distance r_0 to the object. This property of amplitude processing may hinder extraction of breathing and heartbeat realizations. Note that this is a drawback compared to the quadrature processing, where such a dependence is ruled out. The analysis of the absolute values of spectra (13) calculated for different distance phases ($\psi_0 = 0°$, 60°, and 90°) shows that, at $\psi_0 = 0°$, useful components with frequencies 0.23 and 1.10 Hz vanish from the spectrum of the desired signal; only mixed components are preserved. At $\psi_0 = 90°$, we see the appearance of the desired components of the spectrum and the mixed components that are absent at $\psi_0 = 0°$. At intermediate values, for example, at $\psi_0 = 45°$, all possible desired and mixed components are present in the spectrum, which, in this case, almost coincides with the output spectrum of a coherent quadrature receiver (see Fig. 1).

The time realization at the output of the amplitude receiver coincides with one of the output components of the quadrature receiver (see Fig. 2) and contains no first harmonics of breathing and heartbeat at certain values of ψ_0, as predicted by calculations.

2. PROBING LIVE OBJECTS BY VIDEO SIGNAL RADARS

Owing to their high delay resolution, UWB video signals can also be used in short-range radars for detection of signals produced by small motions of a human object, such as breathing and heartbeat signals. Video pulses used in radar sensors have a low average power and can allow through-wall detection of human objects only at short distances (and under the condition that the obstacle is transparent to radio signals). As in the previous consideration of radar sensors with monochromatic unmodulated signals, our aim is to study demodulation methods that allow extraction of biometric signals and analysis of their time–frequency structure at various distances to the object.

As irradiated and reference video signals, we consider the following three types of signals, chosen because of their mathematical simplicity:

$$s_0(t) = \exp(-\alpha_0 t^2)\cos\omega_0 t,$$

$$s_1(t) = \exp(-\alpha_1 t^2)\sin(\omega_1 t), \qquad (14)$$

$$s_2(t) = \exp(-\alpha_2 t^2)[\cos\omega_2 t - \exp(-\omega_2^2/(4\alpha_2))].$$

Note that, in line with the radiation conditions, the time- averaged values of these signals should be equal to zero. This condition is satisfied for signals $s_1(t)$ and $s_2(t)$, but is not satisfied for $s_0(t)$. Figure 3 shows realizations of these signals for the case when their parameters are as follows:

$$\alpha_0 = \alpha_1 = \alpha_2 = \alpha = \Delta f^2,$$
$$\Delta f = f_\text{h} - f_\text{l}, \quad \omega_0 = \omega_1 = \omega_2 = 2\pi\frac{f_\text{h} + f_\text{l}}{2}, \qquad (15)$$

where f_l and f_h are the low- and high-frequency limits of the pulse spectrum (for the signals in Fig. 3, f_l = 0.2 GHz and f_h = 1.8 GHz). For comparison, also plotted is the harmonic signal with the frequency equal to the average frequency of the video pulse. As a rule, probing and reference pulses are repeated with a certain (possibly random) period and repetition rate as high as several megahertz on average.

The specific waveform of pulse $s_1(t)$ resembles the characteristic of a time discriminator. Such video pulses can serve as reference, or strobe, pulses in applications where the time position of pulses reflected from a target should be accurately determined or where demodulation of carried biometric information is required. Pulses of type $s_0(t)$ are suitable reference strobes for the range gating systems. Both waveforms $s_1(t)$ and $s_2(t)$ can be used as models of radiated pulses.

We consider two variants of signal processing: the cross-correlation technique and, as a particular case of it, stroboscopic transformation. In the cross-correlation method, received (s_i) and reference (s_j) signals are multiplied and the result is accumulated in the integrator. Mathematically, the average output of the correlator can be represented in the form of the correlation integral

$$Q_{ij}(\theta_\text{rec}, \theta_\text{ref}) = \int_{-\infty}^{\infty} s_i(t - \theta_\text{rec}) s_j(t - \theta_\text{ref})\,dt, \qquad (16)$$

where θ_{rec} and θ_{ref} are the delays of the received and reference signals, respectively.

In the case of stroboscopic transformation, the output effect is obtained if the reference signal in (16) has the form of the delta function $s_j(t) = \delta(t)$:

$$Q_{i\delta}(\theta_{rec}, \theta_{ref}) = s_i(\theta_{\theta_{ref}} - \theta_{rec}). \quad (17)$$

Integrals (16) depend only on the difference $\tau = \theta_{rec} - \theta_{ref}$ and, for signals (14), can be calculated analytically. Functions $Q_{00}(\tau)$ and $Q_{11}(\tau)$ are even functions of τ, while $Q_{01}(\tau) = Q_{10}(\tau)$ are odd functions. If conditions (15) are fulfilled, $Q_{00}(\tau)$ and $Q_{11}(\tau)$ take the form

$$Q_{00(11)}(\tau) = \sqrt{\frac{\pi}{8\alpha}}\exp(-\alpha\tau^2/2) \times [\cos(\omega_0\tau) \pm \exp(-\omega_0^2/(2\alpha))]. \quad (18)$$

Since they are more cumbersome, similar expressions for $Q_{02}(\tau)$ and $Q_{01}(\tau)$ are omitted here.

Video signals can be received by means of a two-channel time discriminator [17] with the discrimination characteristics

$$D_{00}(\Delta\tau) = \frac{1}{Q_{00}(0)}(Q_{00}(\Delta\tau + \Delta\vartheta) - Q_{00}(\Delta\tau - \Delta\vartheta)), \quad (19)$$

$$D_{02}(\Delta\tau) = \frac{1}{Q_{02}(0)}(Q_{02}(\Delta\tau + \Delta\vartheta) - Q_{02}(\Delta\tau - \Delta\vartheta)), \quad (20)$$

$$D_{2\delta}(\Delta\tau) = \frac{1}{s_2(0)}(s_2(\Delta\tau + \Delta\vartheta) - s_2(\Delta\tau - \Delta\vartheta)), \quad (21)$$

where $2\Delta\theta$ is the time offset of reference strobe pulses s_j in the first and second correlation channels.

Figure 4 presents examples of normalized correlation functions $Q_{ij}(\Delta\tau)$ versus the relative offset $\tau = \theta_{rec} - \theta_{ref}$ between the received and reference signals arriving at the correlator input; the harmonic signal with a frequency equal to the average frequency of the signal spectrum is also shown. Corresponding discrimination characteristics $D_{00}(\Delta\tau)$, $D_{02}(\Delta\tau)$, and $D_{2\delta}(\Delta\tau)$ are plotted in Fig. 5 for the case $2\Delta\theta = \Delta f^{-1}$ when conditions (15) are satisfied, which means that correlation functions $Q_{00}(\Delta\tau)$ and $Q_{11}(\Delta\tau)$ almost coincide. It is seen that the maximum first derivatives of all the normalized correlation functions with respect to $\Delta\tau$ are nearly the same and coincide with the maximum steepness of the unmodulated harmonic signal at the average frequency of the signal spectrum.

The presence and periodicity of the peaks and dips in both cases make it evident that the amplitude reception of unmodulated signals and cross-correlation processing of video-pulse signals face the same problem caused by the presence of mixed and higher harmonics of breathing and heartbeat. The same conclusion can be made regarding the discrimination characteristics. When probing signals are video pulses, mixed and higher harmonics arise at medium distances to a target. These harmonics are unfavorable since the average delay of the signal falls at the maximums of the correlation function or of the discrimination characteristic. The time portrait of the second harmonic of breathing obtained in the cross-correlation method using video-pulse signals is completely similar to that shown in

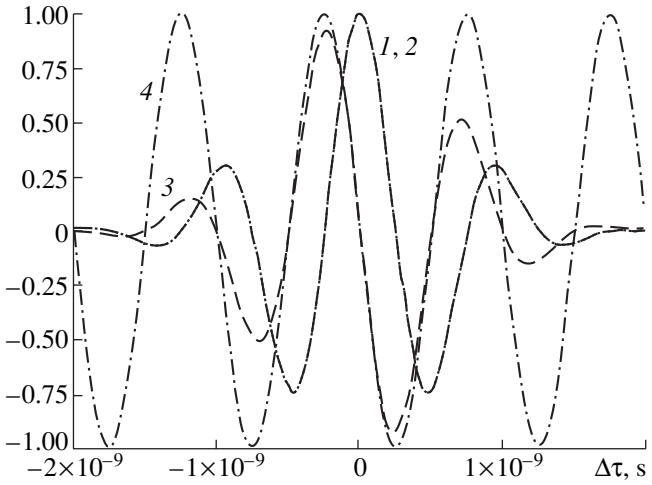

Fig. 4. Normalized correlation functions (*1*) $Q_{00}(\Delta\tau)/Q_{00}(0)$, (*2*) $Q_{11}(\Delta\tau)/Q_{11}(0)$, and (*3*) $\sqrt{8\alpha_0\pi^{-1}}\,Q_{01}(\Delta\tau)$, and (*4*) harmonic function $-\sin(\omega_0\Delta\tau)$ vs. offset $\Delta\tau$ between the received and reference signals.

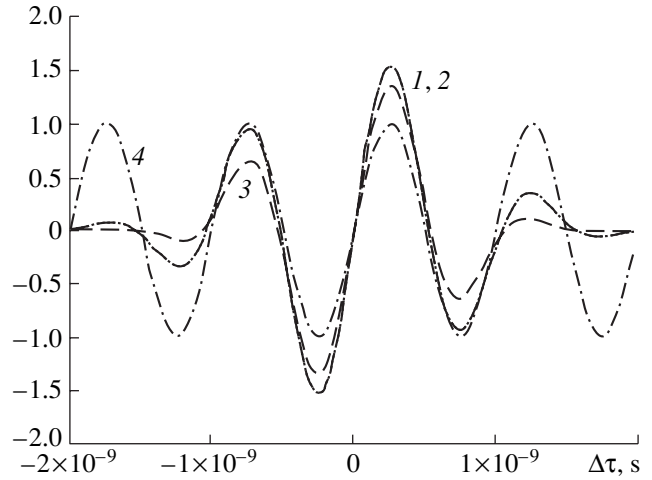

Fig. 5. Discrimination characteristics (*1*) $D_{00}(\Delta\tau)$, (*2*) $D_{02}(\Delta\tau)$, and (*3*) $D_{2\delta}(\Delta\tau)$, and harmonic function (*4*) $\sin(\omega_0\Delta\tau)$ vs. offset $\Delta\tau$ of the received signal from the zero of the discrimination characteristic.

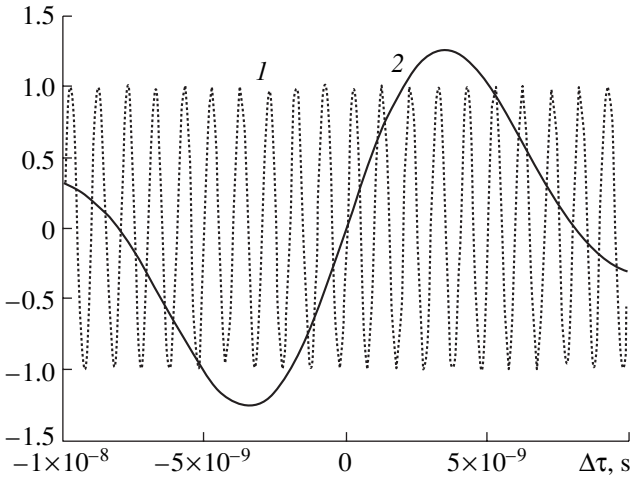

Fig. 6. (*1*) Function $\sin(\omega_0 \Delta t)$ and (*2*) a broad discrimination characteristic $D(\Delta\tau)$ at $2\Delta\theta = 8\Delta f^{-1}$.

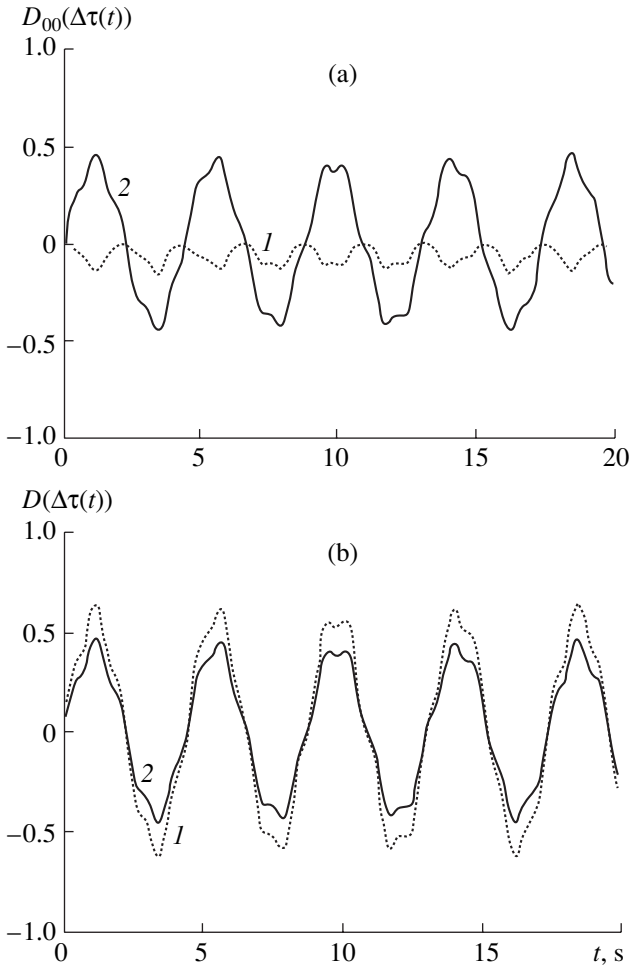

Fig. 7. (*1*) Output realizations of breathing and heartbeat and (*2*) initial deviations of the delay $D(\Delta\tau(t))$ at $\Delta\tau_0 = 0.25$ ns for (a) narrow $D_{00}(\Delta\tau(t))$ and (b) broad $D(\Delta\tau(t))$ discriminator apertures.

Fig. 2 for one quadrature of a monochromatic signal. However, in the case of monochromatic signals, the quadrature processing and phase demodulation entirely eliminate nonlinear distortions of a biometric signal, a result that can hardly be achieved with video-pulse signals. The situation can be improved, for example, by using broader strobe pulses and longer delay $2\Delta\theta$ between them; i.e., by substantially extending the linear section of the discrimination characteristic compared to the case shown in Fig. 5.

Figures 5 and 6 show the outputs of discriminators with broad and narrow discrimination characteristics, $D(\Delta\tau)$ and $D_{00}(\Delta\tau)$, respectively. The increments in the delay due to breathing and heartbeat have been calculated using formulas (2) and (5). Average-centered output realizations of breathing and heartbeat calculated at a nonzero offset of the delay $\Delta\tau_0 = 0.25$ ns from the zero point in a narrow- and wide-aperture discriminators are given in Figs. 7a and 7b, respectively (dotted curves). The solid line shows the initial phase fluctuations, which are proportional to the delay fluctuations.

Comparison of realizations in Fig. 7 suggests that, in a video-pulse sensor with a narrow-aperture discriminator, even small permanent offsets of the delay (distance) from the zero point of the discrimination characteristic may give rise to the second harmonic of breathing and heartbeat, as occurred in a monochromatic sensor with amplitude processing. To eliminate this drawback in a video-pulse sensor directly measuring the delay, the linear section of the discriminator aperture should be at least several times longer.

Along with the methods considered above, there are alternative techniques of demodulation and extraction of undistorted biometric signals. These techniques could also be used in [7, 12], but they were not specially mentioned there. These may be methods where received video pulses are represented as a sequence of pulses with pulse-position modulation (PPM) [19]. In such a sequence, the position (or delay) of received video pulses is modulated by the useful biometric information that can be extracted from the pulse sequence by applying a low-frequency filter or a bandpass filter [19] with its band encompassing the spectrum of breathing and heartbeat frequencies. In order to increase the useful component, which is only small in the case of PPM, we can recommend transforming a PPM signal into a signal with pulse-width modulation (PWM) with the following low-frequency filtering [19]. Analytical calculation of PPM and PWM spectra is a difficult mathematical problem even for harmonic modulation in view of the time variability of the pulse sequence in both cases [19]. Furthermore, demodulation of biometrical information has to be performed for extremely low modulation indices because of low frequencies of breathing and heartbeat and the small relative deviation of pulses $\Delta\tau_{max}/T_r = 2\Delta_{br}/(cT_r)$, which amounts to 6×10^{-5} for $\Delta_{br} = 1$ cm and a typical repetition period of $T_r = 1$ μs. Under these conditions, demodulation of both

PPM and PWM signals yields an almost undistorted spectrum with vanishingly small higher harmonics [19].

For a pulse sequence with a random repetition period, these demodulation methods have not been studied yet. It is clear, however, that demodulation of such a pulse series may lead to additional noise. The possibility of cancelling this noise is offered by cross-correlation processing or by applying time discriminators. Indeed, additional demodulation noise is diminished if the values obtained at the cross correlator or discriminator output are related to equidistant time instants closest to random moments of pulse radiation. Calculation of the spectral density of noise produced upon demodulating a signal sequence with a random repetition period is an independent problem that goes beyond the scope of this study.

One more demodulation method for video signals can be proposed based on range monitoring [17]. This method is especially advantageous for narrow-aperture time discriminators and is similar to phase measurements performed by the tracer ring of an automatic frequency control system in monochromatic-signal radar sensors.

3. EXTRACTION OF BIOMETRIC SIGNALS FROM INTERFERENCE REFLECTIONS IN A RADAR SENSOR WITH STEPWISE FREQUENCY MODULATION

Mathematically, a probing signal with stepwise frequency modulation (SFM) is a sum of $M + 1$ partial frequency components with frequencies ω_m ($m = 0, 1, 2, \ldots, M$) that do not overlap in time and comprise a burst of $M + 1$ pulses with the off-duty factor close to unity [20]. The bursts follow one another with repetition period T_r. A burst of SFM signals radiated during the kth repetition period can be written as

$$\dot{s}_{Tk}(t) = \sum_{m=0}^{M} a_0(t - kT_r - mT_\omega)\exp[j\omega_m(t - kT_r)]. \quad (22)$$

Here, T_r is the repetition period of bursts comprised of $M + 1$ frequency components and T_ω is the frequency step, the same for all the bursts. One-component pulse has a rectangular envelope,

$$a_0(t) = \mathrm{rect}\left(\frac{t}{T_\omega - \tau_{max}}\right), \quad (23)$$

with a duration $\tau_\omega = T_\omega - \tau_{max}$, where $\tau_{max} = 2r_{max}/c$ is the time delay corresponding to the maximum reliable range of the radar sensor. Such a choice of the component pulse duration ensures nonoverlapping component pulses with different frequencies for the reference and received signals within the operation range. Usually, the frequency components are equidistant with a step of

$$\omega_m = \omega_0 + m\Delta\omega, \quad m = 0, 1, 2, \ldots, M. \quad (24)$$

In a matched processing system, the reference signal in the kth period represents a copy of probing pulse (22) but is shifted by a certain expectable delay τ_{ref}:

$$\dot{s}_{refk}(t) = \sum_{m=0}^{M} a_1(t - kT_r - mT_\omega) \times \exp[j\omega_m(t - kT_r - \tau_{ref})], \text{ where } a_1(t) = \mathrm{rect}\left(\frac{t}{T_\omega}\right). \quad (25)$$

Let us generalize model (5) of fluctuations of the delay and phase of a radar signal reflected from a live object. Assume that live and local objects form a system of totally $(N + 1)$ objects with unified numeration characterized by number n, $0 \le n \le N$. Then, the delay and phase of a reflected signal appear, respectively, as

$$\tau_{rec}^{(n)}(t) = \tau_0^{(n)} + \Delta\tau_{rec}^{(n)}(t) = \frac{2}{c}\left[r_{0n} + \Delta_{brn}\sin\left(\frac{2\pi t}{T_{brn}} + \varphi_{brn}\right) + \Delta_{hbn}\sin^{2s}\left(\frac{\pi t}{T_{hbn}} + \varphi_{hbn}\right)\right], \quad (26)$$

$$\varphi_{rec}^{(n)}(t) = -\varphi_{0m}^{(n)} - \Delta\varphi_m^{(n)}(t) = -\frac{2\omega_m r_{0n}}{c} - \omega_m\Delta\tau_{rec}^{(n)}(t). \quad (27)$$

Here, c is the velocity of electromagnetic waves; Δ_{brn}, Δ_{hbn}, T_{brn}, T_{hbn}, φ_{brn}, and φ_{hbn} are the amplitudes, periods, and phases of the breathing and heartbeat signals; and $s > 1$ is an integer parameter of approximation of heartbeat pulses. For quiescent local objects, we put $\Delta_{brn} = \Delta_{hbn} = 0$. In this model, the breathing-induced vibrations of the body surface are also modeled by a sine function and vibrations produced by heartbeat have a pulselike shape as a result of raising the sine to an even degree of $2s$.

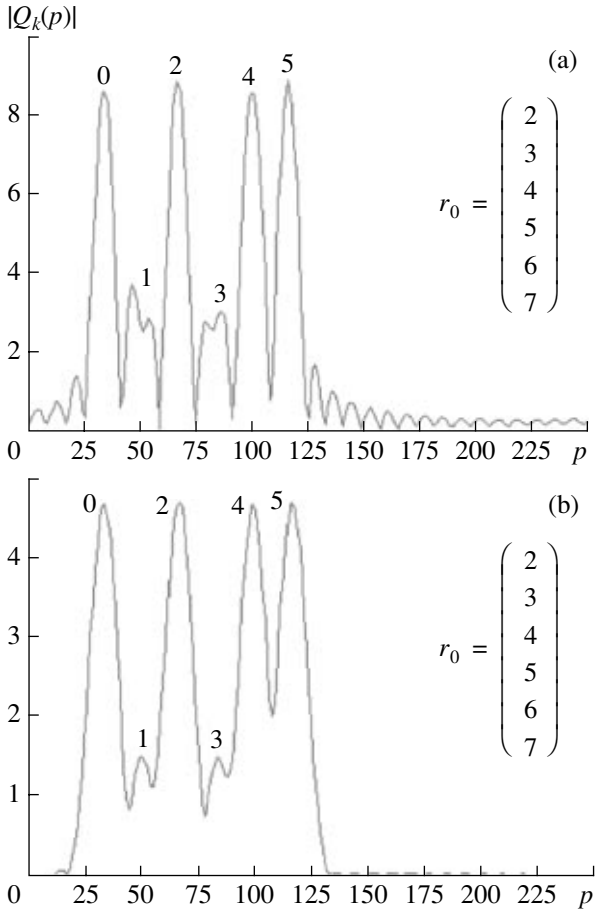

Fig. 8. Range profiles determined from formula (31) for six objects (0–5) at the kth probing period for (a) unweighted and (b) Hamming-weighted frequency components.

Taking into account (26), a signal received after reflection from $N + 1$ objects in the kth probing period can be expressed in the form

$$\dot{s}_{\mathrm{rec}k}(t) = \sum_{m=0}^{M}\sum_{n=0}^{N} q_m^{(n)} a_0 (t - \tau_{\mathrm{rec}}^{(n)}(t - \tau_0^{(n)}/2) - kT_{\mathrm{r}} - mT_{\omega}) \times \exp[j\omega_m (t - kT_{\mathrm{r}} - \tau_{\mathrm{rec}}^{(n)}(t - \tau_0^{(n)}/2))], \quad (28)$$

where factor $q_m^{(n)}$ appears due to reflection and propagation of waves of the mth frequency for the nth object.

To construct the processing algorithm for an SFM signal, we first find the correlation integral in the kth repetition period. In the absence of overlapping between the received and reference component pulses with different frequencies and in view of an insignificant variation in the function $\tau_{\mathrm{rec}}^{(n)}(t)$ over interval T_{ω}, the correlation integral can be written as

$$Q_k(\tau_{\mathrm{ref}}) = \int_{kT_{\mathrm{r}}}^{(k+1)T_{\mathrm{r}}} \dot{s}_{\mathrm{rec}k}(t)\dot{s}^*_{\mathrm{ref}k}(t)dt \approx (T_{\omega} - \tau_{\max}) \sum_{m=0}^{M} \dot{V}_{m,k} \exp(j\omega_m \tau_{\mathrm{ref}}), \quad (29)$$

where

$$\dot{V}_{m,k} = \dot{A}_m(kT_{\mathrm{r}} + mT_{\omega} + 0.5(T_{\omega} - \tau_{\max})),$$
$$\dot{A}_m(t) = \sum_{n=0}^{N} q_m^{(n)} \exp\{-j\omega_m \tau_{\mathrm{rec}}^{(n)}(t + \tau_0^{(n)}/2)\}, \quad (30)$$

and $\tau_{\mathrm{rec}}^{(n)}(t)$ and $\tau_0^{(n)}$ are defined in (26).

Using (24) and the equality $\omega_m = 2\pi f_m = 2\pi m\Delta f + 2\pi f_0$ and replacing continuous delay τ_{ref} by discrete variable p ($p = 0, \ldots, M$) according to the formula $\tau_{\mathrm{ref}} \approx p[(M + 1)\Delta f]^{-1}$, we reduce (29) to the form of a discrete Fourier transform [16]:

$$\dot{Q}_k(p) = (T_{\omega} - \tau_{\max}) \exp\left(j\frac{2\pi f_0 p}{(M+1)\Delta f}\right) \times \sum_{m=0}^{M} \dot{V}_{m,k} \exp\left(j\frac{2\pi}{(M+1)}(mp)\right), \quad (31)$$

which can be computed using the standard fast Fourier transform (FFT) procedure.

The spectral components of breathing and heartbeat can be revealed by further processing of data obtained in scans $k = 0, \ldots, K$ over a long observation interval KT_{r}. This processing can be performed by applying the FFT to $\dot{Q}_k(p)$ in terms of discrete variable k for each particular distance cell p:

$$\dot{S}(p, q) = \sum_{k=0}^{K} \dot{Q}_k(p) \exp\left(j\frac{2\pi}{(K+1)}qk\right) = FFT_k\{\dot{Q}_k(p)\}. \quad (32)$$

As a result, we obtain a 2D delay–frequency matrix ($S_{p,q} = |\dot{S}(p, q)|$) in the plane of distance cell number p and spectral component number q. In this matrix, the responses from fixed local objects located at different distance cells are found at zero and close to zero components at $q = 0, 1$. In contrast, responses of live objects contain components at $q \geq 2$, which correspond to the breathing and heartbeat frequencies and their harmonics.

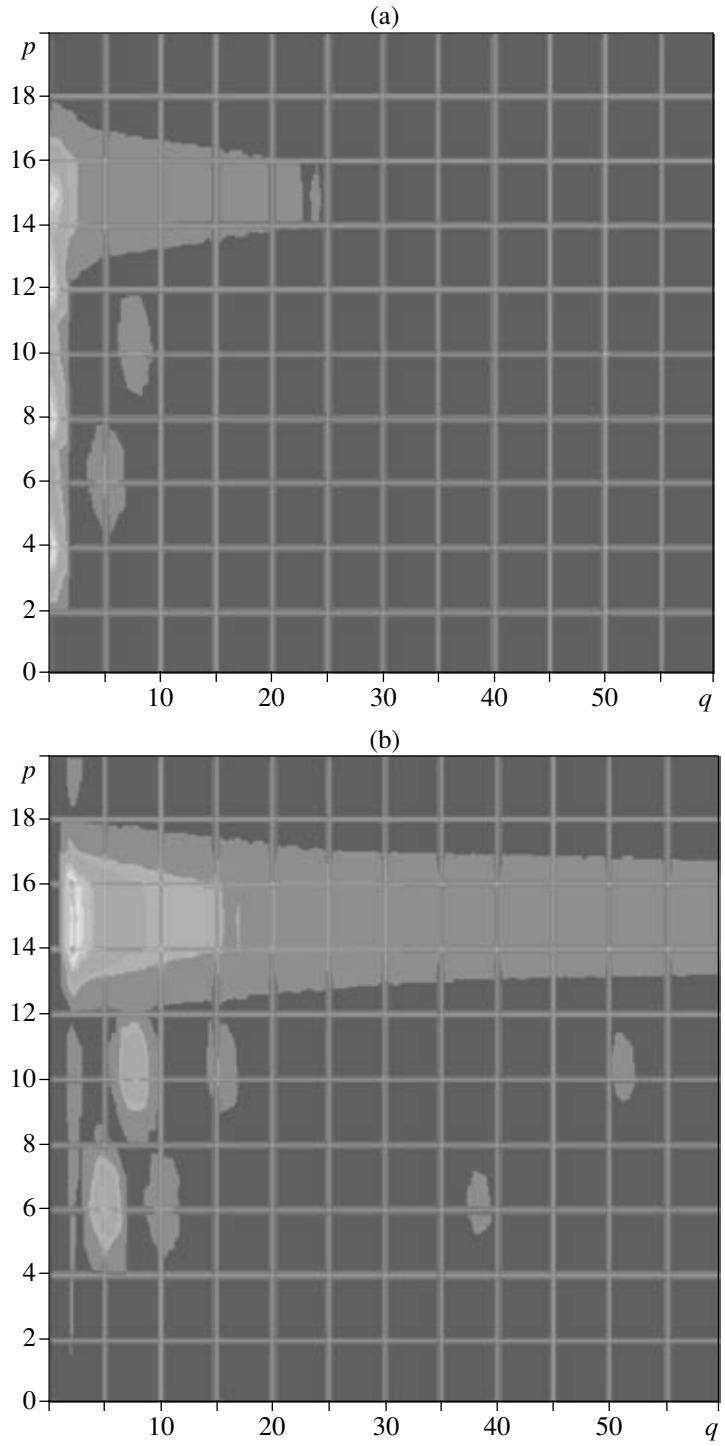

Fig. 9. Topographic frequency–range diagrams $|\dot{S}(p, q)|$ for the considered system of objects (a) without rejection and (b) with frequency rejection of local objects; q is the frequency sample and p is the distance cell.

By way of example, consider the results of calculation based on model (29)–(32) for detection of breathing and heartbeat in a radar sensor with the following parameters: the initial frequency of SFM signal f_0 = 2.0 GHz, the bandwidth ΔF = 300 MHz (for the range resolution δr = 0.5 m), the number of frequency steps $M + 1 = 32$, the frequency step $T_\omega = 312.5$ μs, the burst repetition period $T_r = 25$ ms, the number of bursts $K + 1 = 1024$, and the total observation period $KT_r = 25.6$ s. Totally, six objects ($N + 1 = 6$) with the unified numeration $n = 0, 1, \ldots, 5$ are spaced from the radar at the respective distances r_{0n} = 2, 3, 4, 5, 6, and 7 m. The

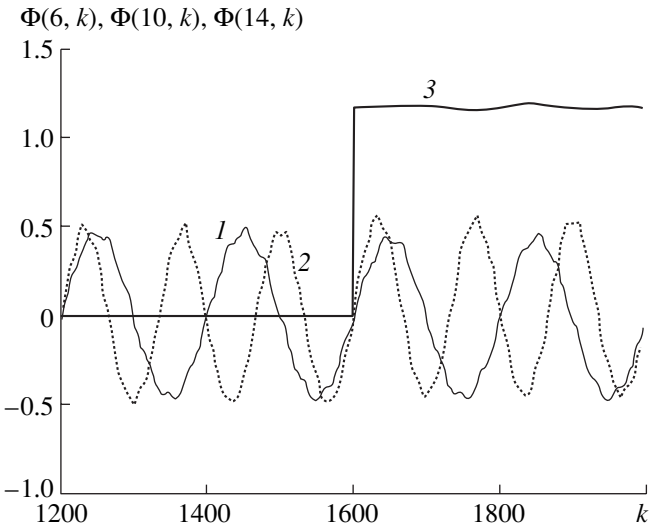

Fig. 10. Breathing and heartbeat realizations in the (*1*) sixth and (*2*) tenth distance cells for the case of (*3*) a stepwise transition of the sixth object from the 14th to 15th cell.

objects with $n = 0$, 2, and 4 located at the distances 2, 4, and 5 m from the radar are fixed local objects with a radar cross section (RCS) of 10 m^2. The object with the number $n = 5$ located at a distance of 7 m has the same RCS and simulates an instant transition from its own distance cell into the next cell in the direction away from the radar. Objects $n = 1$ and 3 simulate two live objects for the case when the skin pattern of the area equal to RCS = 1 m^2 moves and the breathing and heartbeat frequencies are as follows: $F_{\text{br1}} = T_{\text{br1}}^{-1} = 0.2$ Hz, $F_{\text{br3}} = T_{\text{br3}}^{-1} = 0.3$ Hz, $F_{\text{hb1}} = T_{\text{hb1}}^{-1} = 1.5$ Hz, and $F_{\text{hb3}} = T_{\text{hb3}}^{-1} = 2.0$ Hz. The displacement amplitudes are $\Delta_{\text{br1}} = \Delta_{\text{br3}} = 0.5$ cm and $\Delta_{\text{hb1}} = \Delta_{\text{hb3}} = 0.5$ mm, respectively.

Figure 8 shows the range profiles at a certain time moment that are determined as the absolute value of the correlation integral calculated on the basis of formula (31) for a sequence of 32 frequency samples completed with zero values up to 256 samples for the sake of smoothing the profiles. The procedure has been carried out for both unweighted frequency components (Fig. 8a) and the components weighted using an ordinary Hamming window [16] (Fig. 8b). Numerals are the numbers of the objects, while the components of the vector represent the distances to the objects measured in meters.

Figure 9 presents the result of modeling in the form of topographic diagrams plotted for the absolute values of the delay–frequency matrix elements, $S_{p,q} = |\dot{S}(p, q)|$. The data obtained at different frequencies are weighted by the Hamming method. Figure 9a corresponds to the calculation without frequency rejection of the local objects; and Fig. 9b, to the case when the simplest type of frequency rejection is applied: after applying the FFT, the zeroth and first frequency samples (where the responses of the local objects are concentrated) are set equal to zero in all the distance cells. The spectrum corresponding to a stepwise change in the phase of the most distant object with $n = 5$ that jumps between two neighboring distance cells is not completely rejected in view of its broadness.

However, range selection still works for this object and the object's signals do not suppress the spectral components of breathing and heartbeat of the live objects with the numbers $n = 1$ and 3 at the distances 3 and 5 m. It is seen that suppression of the signals reflected from local objects improves detection of heartbeat components near frequency samples with numbers of $q = 38$ and 52. The maxima observed in the vicinity of the samples with $q = 5$ and 7–8 correspond to the breathing frequencies of the same subjects and grow as a result of rejection. The topographic diagram in Fig. 9b shows the second harmonics of breathing. The mixed and higher harmonics of breathing and heartbeat are not seen in the diagram in view of their low intensity.

Analysis of data in the frequency–range plane allows one to determine the distance cell that contains a particular live object. By "focusing" algorithm (31) at this cell, it is possible to separate the time realization of breathing and heartbeat of the object located in the pth cell in accordance with the expression

$$\Phi(p, k) = \arg \dot{Q}_k(p), \quad k = 0, \ldots, K. \qquad (33)$$

In order to avoid phase discontinuities that may occur at the points $\pm\pi$ in (33), it is recommended to use the phase-unwrapping procedure, which, in particular, is described in [21]. Then, the extracted realizations are accurate to a constant component and a constant factor, which are determined by the distance to the object and the method of converting displacements $\Delta_{\text{br}n}$ and $\Delta_{\text{hb}n}$ into phase (33).

Figure 10 presents the reconstructed realizations of heartbeat and breathing of two human objects located in the sixth and tenth distance cells under the conditions of Fig. 9b over a time interval lasting from the 30th to 50th second. The interval is purposely taken symmetric about the time moment $t_s = 40$ s, at which the object with $n = 5$ transits into the next cells at 7.5 m. The reconstructed realizations of breathing and heartbeat are almost undistorted and in good agreement with the variations of phase of the reflected signal calculated from (26) for one of the frequency components. It was noticed that the presence of a discontinuity in a cell spaced far away from the live objects leads to an insignificant rise of the desired signal from the nearest live object. The modeling also has shown that, the closer the cells with live objects to a moving noise source, the stronger their mutual influence. In addition, it has been found that, if the average distance to the live object varies within one distance cell, realizations of breathing

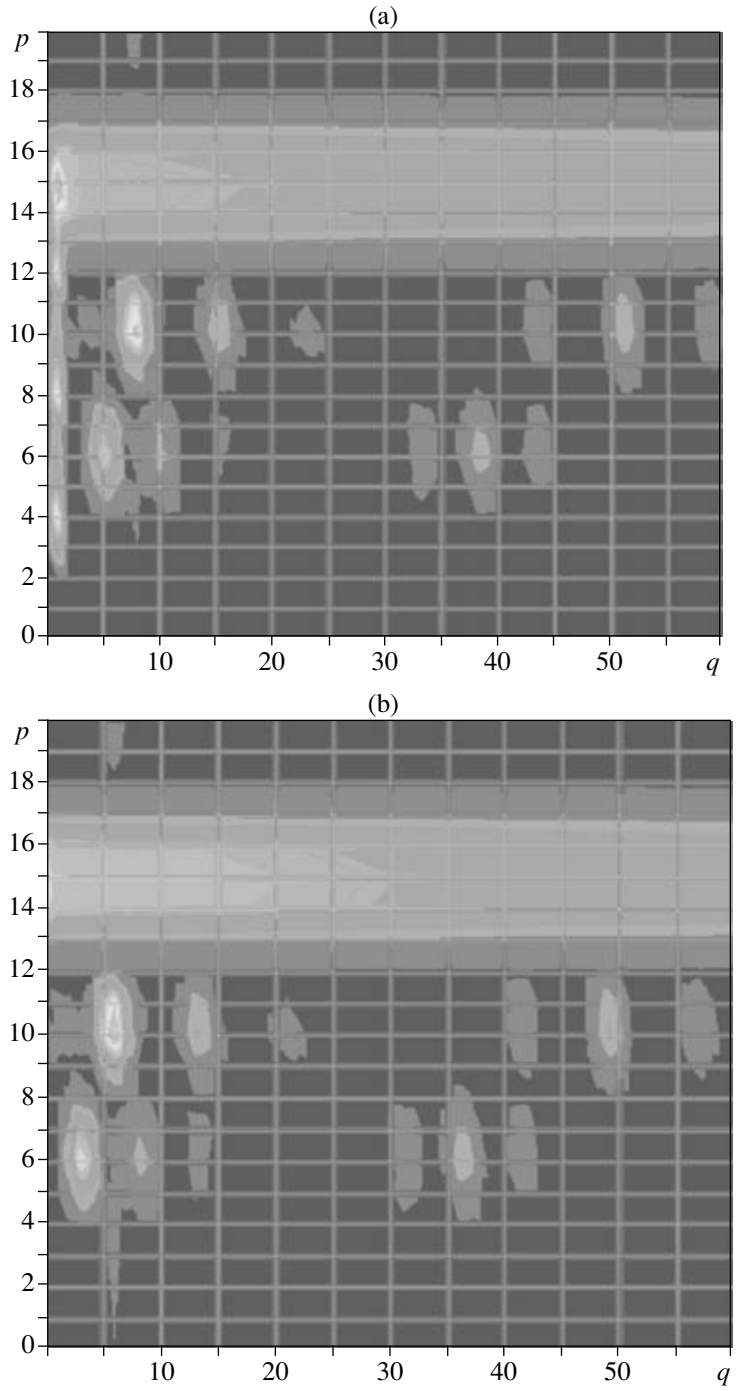

Fig. 11. Topographic frequency–range diagrams for the considered system of objects with rejection (a) only in the time domain and (b) in the time domain combined with additional frequency rejection.

and heartbeat are reliably obtained and the intensity of the second harmonic of breathing is only low. At larger variations of the average distance, a neighboring cell that provides for a minimum distortion upon demodulation should be considered.

The presented method of rejection in the frequency domain is applicable for a sufficiently wide dynamic range of the receiver and a large number of digits in the analog-to-digital converter (ADC). In the case of an insufficient dynamic range (usually, in the presence of intense reflections from local objects), it may be helpful to perform a preliminary instrumental analog processing of reflected signals for each of the quadrature components and for each frequency component f_m [11]. Indeed, let simple analog high-pass filters with time constants τ_f be used to eliminate constant components

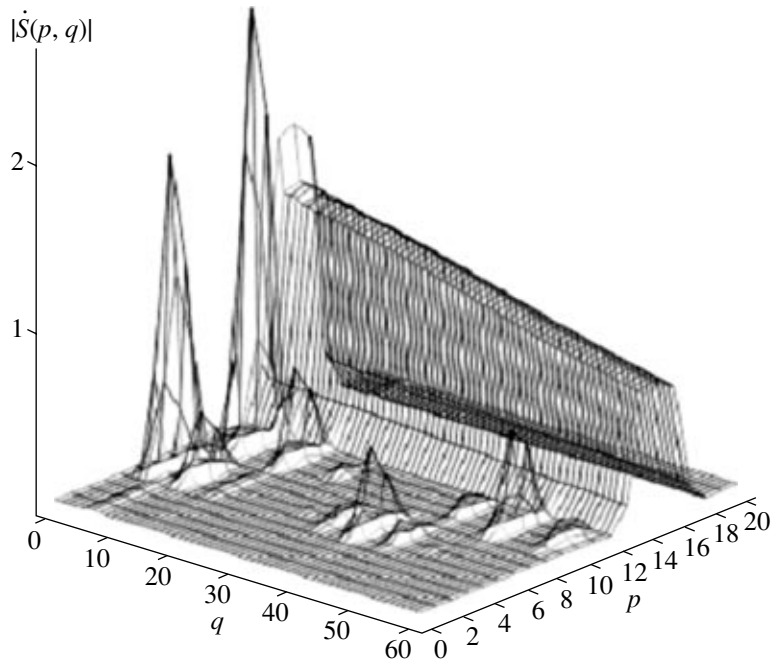

Fig. 12. 3D frequency–range diagram corresponding to the conditions of Fig. 11b.

of highly intense signals from local objects. Time constant τ_f of the filter characterizes the duration of the transient process during which the processing system is focused to the range and the output signal may be distorted. If value τ_f is much smaller than total time of observation KT_r, these distortions are small. In the simulation, each analog filter was represented by its discrete equivalent. Samples from the filter outputs were processed further with the use of the FFT similarly to (31) and (32).

The topographic and 3D diagrams in Figs. 11 and 12 present the results of modeling with the use of rejection in the time domain. The time constant of the filter was taken equal to $\tau_f = 0.1$ s. It is seen from Figs. 9b and 11a that, when rejection in the time domain was used, the ratio between the maximum intensities of heartbeat and breathing is appreciably higher compared to the analogous ratio in the simple variant of frequency rejection. This rise in the intensity stems from the particular choice of the time constant of rejection filters and their frequency characteristics, at which the breathing component is partially suppressed and, therefore, the heartbeat components are relatively enhanced. Figure 11b shows the result of successive application of time rejection and frequency rejection. This procedure consists in removing the zeroth and first frequency samples. Note that the application of frequency rejection alone but with the use of a smoother and more thoroughly selected profile of the filter transfer constant provides for reconstruction of breathing and heartbeats similar to that obtained using time rejection at partial frequency components. However, as mentioned above, such an approach usually lacks the dynamic range of a processing system up to the point where a signal enters the FFT unit.

Similar results related to detection of live objects and extraction of heartbeat and breathing realizations were obtained in [20], where we simulated chirp-radar operation. After reflection from targets, the delayed chirp signals were processed by quadrature detectors separating the difference-frequency component, which successively was Fourier-transformed into instant (at a given chirp-signal period) complex range profiles. Then, a set of complex profiles related to a large number of signal periods was processed for each distance cell, i.e., for each difference frequency, over the entire observation time in which a large number of the chirp periods were measured. As before, the processing of profiles included the FFT and yielded a frequency–range matrix similar to that used in the case of SFM signals.

Along with these similarities, there are significant differences in the practical use of chirp and SFM signals for detection of objects making small motions against intense interfering reflections from local objects. The first distinction is that it is often difficult to obtain a chirp signal with a required highly linear frequency modulation, while generation of SFM signals by a synthesizer of coherent frequencies is instrumentally simple. Another and even more important advantage of applying SFM signals is the possibility to realize in a hardware environment a system of effective rejection of intense reflections from local objects, separately at each of the partial frequencies. This possibil-

ity substantially reduces requirements to the dynamic range of the receiver and to the digital capacity of the ADC compared to the case of using chirp signals.

CONCLUSIONS

Short-range radars intended for detection of people by their breathing and heartbeat may use probing signals of different types. Applicable signals differ mostly in bandwidth. For example, unmodulated monochromatic signals, UWB video pulses, and wideband SFM signals can be employed. The main advantage of wideband and ultrawideband signals over monochromatic signals is that they allow the range separation of targets from exterior interference, such as reflections from local objects and objects making small motions if they are located in distance cells other than those containing a human object.

A significant advantage of continuous wideband SFM signals over UWB video pulses is a higher average power of radiation and, therefore, a longer probing range and higher through-obstacle-penetration power of a radar system for the same level of spatial resolution.

It has been found that, in a monochromatic radar, the time realization and amplitude spectrum of an extracted biometric signal strongly depend on the type of signal processing in the receiver. In the case of coherent quadrature processing, the received signal spectrum does not depend on the distance to a human object and contains the true, multiple, and mixed harmonics of the breathing and heartbeat frequencies as a consequence of natural phase modulation of a signal by the corresponding vibrations of human skin and internal boundaries. The spectral composition of each quadrature component taken separately, as well as the spectral composition of the signal at the output of the amplitude receiver (also containing mixed frequencies), strongly depends on the distance to a human object (the distance phase). It is remarkable that there are some periodically repeating distances (injured zones) at which the spectrum of the quadrature component and the amplitude spectrum of the signal do not contain true biometric frequencies but include only mixed harmonics. For this type of probing signals, undistorted demodulation of a biometric signal should be based on available methods of phase demodulation; a simple example for use at low noise levels is extraction of two quadratures of the complex envelope of a received signal and calculation of the corresponding phase (argument of the complex envelope minus its time- averaged value) at discrete time instants.

Analysis of the applicability of UWB video pulses for detection of live objects also has revealed the presence of injured zones associated with the dependence of the correlation integral on the delay of the received pulse with respect to the reference pulse. Among possible methods to eliminate injured zones are (i) application of a delay tracking system with a desired lag effect or (ii) the use of time discriminators with a wide linear section in the discrimination characteristic. Such characteristic can be achieved when a signal is received by two correlation channels offset in delay and gated by reference pulses of a special waveform that have a duration much longer than that of the received pulses. In view of the high repeatability of the period in a received sequence of video pulses, it is possible to demodulate almost without distortions a pulse series where the pulse position is modulated in terms of its phase or width. To extract useful data, it suffices to subject the pulse series to low-pass or bandpass filtering with limiting frequencies encompassing the frequency band of biometric signals.

Finally, the characteristics of radars with range selection on the basis of SFM signals have been examined. We have modeled signal-processing algorithms that allow for phase modulation of frequency components by displacements of the human-body surface as a result of breathing and heartbeat. The results of modeling confirm that the spectral components of breathing and heartbeat can be separated from reflections coming from quiescent and slowly moving local objects by means of range gating and 2D fast-Fourier transformation. Two variants of the target selection from the background of reflections are analyzed: (i) selection in the frequency domain by means of a rejecting filter with a rectangular frequency characteristic and (ii) selection in the time domain by applying analog or digital high-pass filters to each frequency channel for every quadrature component. If the time constant of the filter is small, this method provides an additional useful effect: attenuation of breathing components and relative amplification of heartbeat components. The final result of processing a signal reflected from live objects in radars with SFM signals and range gating is extraction of breathing and heartbeat signals in the distance cell containing a live object. The undistorted output signal is the argument (phase) of the complex correlation integral being a function of discrete time, or the probing period, in the distance cell where a live object has been detected.

ACKNOWLEDGMENTS

This work was supported by the Ministry of Education and Science of the Russian Federation, program RNP.2.1.2.1655, and the Russian Foundation for Basic Research, project no. 04-02-08035.

REFERENCES

1. E. F. Greneker, Proc. SPIE: Radar Sensor Technology II **3066**, 22 (1997).
2. E. F. Greneker, in *IEE Conf. RADAR-97, Edinburgh, UK, Oct. 14–16, 1997* (IEE, London, 1997), Vol. 449, p. 150.

3. J. F. Holzrichter, G. C. Burnett, L. C. Ng, and W. A. Lea, J. Acoust. Soc. Am. **103** (1), 622 (1998).
4. Chen Kun-Mu, Huang Yong, Zhang Jianping, and A. Norman, IEEE Trans. Mil. Electron. **27**, 105 (2000).
5. M. A. Barnes, S. Nag, and T. Payment, Proc. SPIE **4374**, 66 (2001).
6. E. M. Staderini, IEEE Aerosp. Electron. Syst. Mag., No. 1, 13 (2002).
7. I. J. Immoreev and S. V. Samkov, Radio Physics and Radio Astronomy (Ukraine) **7** (4), 404 (2002).
8. A. S. Bugaev, I. A. Vasil'ev, S. I. Ivashov, et al., Radiotekhnika, No. 7, 42 (2003).
9. A. S. Bugaev, V. V. Chapursky, S. I. Ivashov, et al., in *Proc. 10th Int. Conf. on Ground Penetrating Radar (GPR 2004), Delft, The Netherlands, June 21–24, 2004*, Ed. by E. C. Slob, A. G. Yarovoy, and J. B. Rhebergen (IEEE, Piscataway, NJ, 2004), Vol. 1, p. 291.
10. A. S. Bugaev, V. V. Chapursky, and S. I. Ivashov, in *Record 2005 IEEE Int. Radar Conf., Arlington, Virginia, May 9–12, 2005* (IEEE, Piscataway, NJ, 2005), p. 359.
11. A. A. Vertiy, I. V. Voinovskyy, and S. Ozbek, in *Proc. Int. Workshop on Microwaves, Radar and Remote Sensing (MRRS-2005), Kiev, Ukraine, Sept. 19–21, 2005* (IEEE, Piscataway, NJ, 2005).
12. A. I. Chernenko and S. V. Samkov, in *Ultrawide-Band Signals and Ultrawide-Band Pulses in Radar, Communications, Acoustics (Rep. 1st Int. Conf., Suzdal', Russia, Sent. 27–29, 2005* (Svyaz', Moscow, 2005), p. 51.
13. D. A. Usanov, Al. V. Skripal', An. V. Skripal', et al., Biomed. Tekhnol. Radioelektron., Nos. 11–12, 44 (2005).
14. *Ultra-Wideband Radar Technology*, Ed. by J. D. Taylor (CRC, Boca Raton, 2000).
15. W. R. Scott, C. Schroeder, and J. S. Martin, Proc. SPIE.: Part of the SPIE Conf. on Detection and Remediation Technologies for Mines and Minelike Targets III **3392**, 176 (1998).
16. L. R. Rabiner and B. Gold, *Theory and Applications of Digital Signal Processing* (Prentice-Hall, Englewood Cliffs, NJ, 1975; Mir, Moscow, 1981).
17. S. V. Pervachev, A. A. Valuev, V. M. Chilikin, et al., *Statistical Dynamics of Radio Trackers* (Sovetskoe Radio, Moscow, 1973) [in Russian].
18. I. A. Vasil'ev, S. I. Ivashov, and V. N. Sablin, Radiotekhnika, No. 4, 55 (1998).
19. Yu. P. Borisov and P. I. Penin, *Principles of Multichannel Data Transmission* (Svyaz', Moscow, 1967) [in Russian].
20. D. R. Wehner, *High Resolution Radar* (Artech House, Norwood, 1987).
21. V. N. Vasil'ev and I. P. Gurov, *Computer-Aided Signal Processing Applied to Interferometric Systems* (BHV, Düsseldorf, 1998) [in Russian].